JPE 2-3-1

A Maximum Power Point Tracking Control for Photovoltaic Array without Voltage Sensor

Tomonobu Senjyu*, Tomiyuki Shirasawa, and Katsumi Uezato

University of the Ryukyus, Okinawa, Japan

ABSTRACT

This paper presents a maximum power point tracking algorithm for Photovoltaic array using only instantaneous output current information. The conventional Hill climbing method of peak power tracking has a disadvantage of oscillations about the maximum power point To overcome this problem, we have developed an algorithm that will estimate the duty ratio corresponding to maximum power operation of solar cell The estimation of the optimal duty ratio involves, finding the duty ratio at which integral value of output current is maximum. For the estimation, we have used the well know Lagrange's interpolation method. This method can track maximum power point quickly even for changing solar isolation and avoids oscillations after reaching the maximum power point.

Keywords: Maximum power point tracking, Output current, Analog integral circuit, PV system

1. Introduction

Recently, since the global environmental problem is worsening, the research and development for the natural energy is actively progress around the world Photovoltaic array system has been a focus of attention for residential photovoltaic energy system because solar cell can directly convert solar energy to electric energy[1] Solar cell has the optimum operating point, and if the PV array operates at this point gives its maximum power output But this optimum operating point of solar cell varies with load, solar insolation, and temperature. Thus, maximum power point tracking (MPPT) control is required to extract maximum power from the solar cell for all conditions

Manuscript received January 8, 2002, revised June 5, 2002
Corresponding Author b985542@tec u-ryukyu ac jp, Tel +81-98-895-8686, Fax +81-98-895-8708

Several methods are proposed for MPPT[2-6]. In general, the MPPT control is implemented using the output power information This output power information is obtained using voltage, current sensors and low-pass filter

Therefore, it leads to complex construction and increases the cost of PV system Further, the conventional MPPT methods use Hill climbing algorithm for maximum power tracking This Hill climbing method tracks the maximum power point by incrementing the duty factor by constant values The disadvantage of this method is that it takes more time to track the maximum power point and the operating point oscillates even after the maximum power point is reached To overcome these problems we proposes a new MPPT algorithm of photovoltaic array using instantaneous output current information. Because in regulated bus PV systems[6], the power output is proportional to the output current Therefore the MPPT can be in implemented by finding the integral value of output current (average value) rather than output power

information The integral value of output current is obtained by a simple integral circuit In this new MPPT algorithm, the optimum operating point is estimated using the Lagrange's interpolation method The proposed method also works well even if solar insolation changes rapidly Performance of the proposed method is compared with that of Hill climbing method through experimental results.

2. Configuration of PV system

The proposed MPPT is implemented using only instantaneous output current information. Configuration of the PV system is shown in Fig 1 Photovoltaic array and battery specifications are shown in Tables 1 and 2, respectively The proposed PV system consists of a two-phase DC-DC boost converter. The converter switches operate with phase difference ϕ of 180° and a switching frequency of 20kHz Integral value of output current V_{int} is the output through an integral circuit shown in Fig. 1, and is detected through an A/D converter The integral circuit diagram used in experiment is shown in Fig. 2.

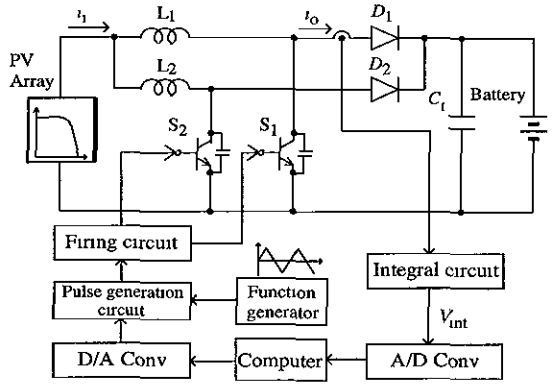

Fig 1 Configuration of PV system

Table 1 Photovoltaic array specification

Maximum power (PMAX)	48.0 W
Open circuit voltage (VOC)	20.7 W
Short circuit current (ISC)	3 10 A
Operating voltage at maximum power	16.7 V
Operating current at maximum power	2 88 A
Module efficiency	1 0 %

(AM1 5, 1000W/m^2, 25°C)

Table 2 Battery specification

Rating voltage	12 0V
Rating capacity	28 Ah

The detailed integral circuit consists of three analog switches, main integral circuit, sample-hold circuit, and a voltage-buffer circuit The integral circuit operates at interval of flowing output current i_o. Time-chart diagram for the integral circuit is shown in Fig. 3 The output current i_o when S_1 of the converter in Fig 1 is off While S_1 is off, SW1 is turned on Then both SW2, SW3 are off It means that the output current i_o is integrated by the integral circuit with SW1 on Next, when S_1 of the converter is turned on, the SW1 is turned off and the SW3 is turned on Then the output voltage of the integral circuit in Fig 2 is transferred to the c_2 capacitor in Fig 2 by SW3. The on period of SW3 is 6μsec It is created by TTL IC 74LS123 with using the on/off signal of S_1 of the converter. After that, SW2 is turned on The on period of SW2 is 6μsec SW2 is the reset switch for the c_1 capacitor. It means that the integrated the output current i_o again

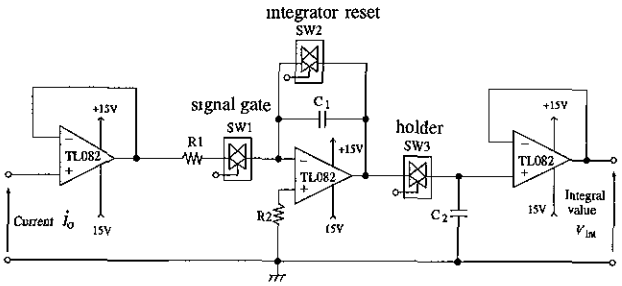

R1, R2 1kΩ, C_1, C_2 8200pF, SW1, SW2, SW3 M4066BP

Fig 2 Integral circuit

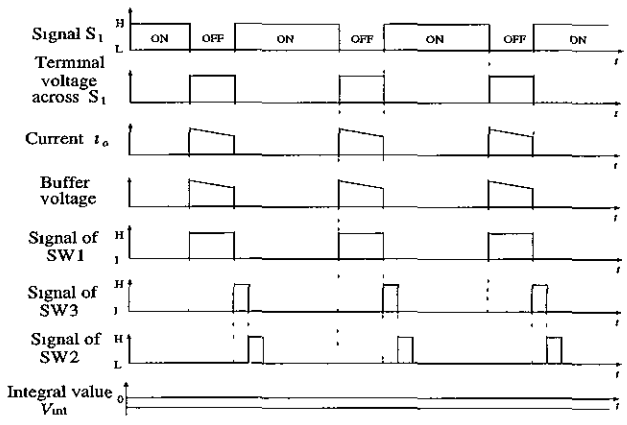

Fig 3 Time-chart diagram.

When duty factor changes from 0 to 1, the output power characteristics of PV array for two different solar insolations are shown in Fig 4 and the integral value of output current characteristics are also shown in Fig 5 It is evident that the solar cell has the optimum operating point at which it gives maximum power Then the integral value of output current also changes in the same fashion as that of output power. Since the integral value of output current is proportional to the output power of PV array, it is possible to track the maximum power point of PV array using only the output current information instead of output power information

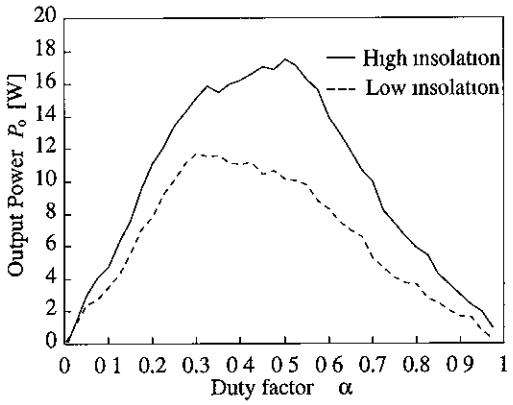

Fig 4 P_o versus α

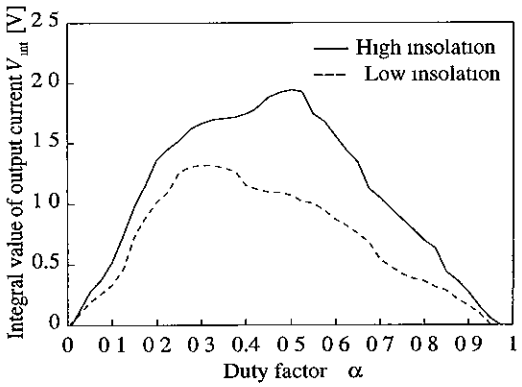

Fig 5 V_{int} versus α

3. Maximum power point tracking control

In MPPT control, to obtain a good tracking performance, the duty factor $\hat{\alpha}_{opt}$ corresponding to maximum power point of the PV array is estimated based on V_{int} characteristic curve approximation using Lagrange's interpolating method. The estimated value of duty ratio $\hat{\alpha}_{opt}$ converter tracks the maximum power point. Further, the operating point of PV array reaches the maximum power point quickly and will not make any oscillations about this maximum power point The tracking method is described in the following steps.

Step 1: When duty factor is α = 0.1, 0.2, 0.3,..., 0.7, determine corresponding integral values of output current V_{int} . These values let say $V_{int} = V_{int1}, V_{int2}, V_{int3}, \ldots, V_{int7}$.

Step 2 The integral value of output current between the values determined as in STEP1 is estimated by using Lagrange's interpolation method. The estimated V_{int} is defined as $\hat{V}_{int}$

The first Lagrange interpolation

To estimate V_{int} from α = 0.1 to α = 0 4, $\hat{V}_{int}$ is estimated in the intervals of incremental duty ratio $\Delta\alpha$ = 0.02 by using the already known V_{int} $\hat{V}_{int}$ is calculated by using the following equation,

$$\begin{aligned}\hat{V}_{int} = &\frac{(x-x_1)(x-x_2)(x-x_3)}{(x_0-x_1)(x_0-x_2)(x_0-x_3)}y_0 \\ &+\frac{(x-x_0)(x-x_2)(x-x_3)}{(x_1-x_0)(x_1-x_2)(x_1-x_3)}y_1 \\ &+\frac{(x-x_1)(x-x_2)(x-x_3)}{(x_2-x_0)(x_2-x_1)(x_2-x_3)}y_2 \\ &+\frac{(x-x_1)(x-x_2)(x-x_3)}{(x_3-x_0)(x_3-x_1)(x_3-x_2)}y_3\end{aligned} \quad (1)$$

where, x is α estimated, and $(x_0, y_0) = (\alpha_{01}, V_{int1})$, $(x_1, y_1) = (\alpha_{02}, V_{int2})$, , $(x_3, y_3) = (\alpha_{04}, V_{int4})$

The second Lagrange interpolation

To estimate V_{int} from α = 0 4 to α = 0.7, $\hat{V}_{int}$ is estimated at intervals of incremental duty ratio $\Delta\alpha$ = 0 02 by the detected V_{int} $\hat{V}_{int}$ is calculated by the above equation (1) Fig. 6 shows the result of Lagrange's interpolation method for high solar insolations As shown in Fig. 6, the $\hat{V}_{int}$ estimated is exactly matching with that obtained in Lagrange's interpolation.

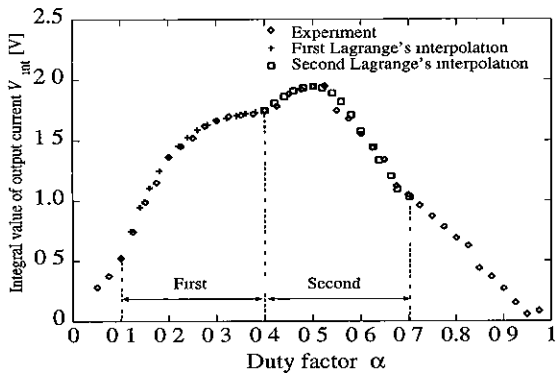

Fig 6 The results of the Lagrange's interpolation for high insolation

Step 3 Select maximum V_{int} which has a maximum value in the above estimated $\hat{V}_{int}$ and the detected V_{int} The selected V_{int} is defined as $\hat{V}_{imax}$ Then, $\hat{\alpha}_{opt}$ which has $\hat{V}_{imax}$ is defined as duty ratio corresponding to maximum power point The experimental setup adjusts the duty ratio to $\hat{\alpha}_{opt}$ and tracks the maximum power point.

Step 4 The estimation error is determined by the following equation,

$$| \hat{V}_{imax} - V_{int} | = 0.10 \text{ (V)} \quad (2)$$

where, $\hat{V}_{imax}$ is the selected V_{int} by *Step*3 V_{int} is actual integral value of output current corresponding to $\hat{\alpha}_{opt}$

If the estimated error satisfies equation (2), it appears that the maximum power point of PV array is reached by using $\hat{\alpha}_{opt}$ Then, *Step*4 is repeated, using its $\hat{\alpha}_{opt}$ It means that this method can avoid oscillations after reaching the maximum power point. When the estimated error is not satisfied equation (2), the error is considered big Then it necessary to go back to *Step1*, because it means that $\hat{\alpha}_{opt}$ is not corresponding to the maximum power point Equation (2) represents the evaluation of the estimated error. In case of variable solar insolation if equation (2) is not satisfied, go to *Step*1, because it appears that solar insolation changes suddenly. Based on the above algorithm, the maximum power point tracking is implemented experimentally.

4. Experimental Results

To examine the effectiveness of the proposed MPPT methods, experimental results are presented for constant and stepwise insolations. In the experiment, the performance of the proposed algorithm using the Lagrange's method and the proposed MPPT using instantaneous output current are compared with the Hill climbing method, where the sampling periods are 8 msec, respectively The initial duty factor $\alpha_0 = 0.1$, the incremental (or decremental) duty factor $\Delta\alpha$ in the Hill climbing method is 0 05

4.1 Experimental Results for High Solar Insolation

The performance of MPPT at high solar insolation is shown in Fig 7 Figs 7(a), 7(b), and 7(c) show the output power, integral value of output current V_{int}, and duty factor α, respectively From the output power shown in Fig. 7(a), the proposed method tracks the maximum power point quickly, which is the same as the result obtained from the Hill climbing method It shows that optimum operating point $\hat{\alpha}_{opt}$ is exactly estimated in Fig 7(c), where $\hat{\alpha}_{opt}$ is close to 0 52 Since it can estimate $\hat{\alpha}_{opt}$ in the seven data point, it will take about 56 msec for tracking the maximum power point From Fig 7, it can be noticed that the proposed algorithm reaches the maximum power point and tracks continuously without any oscillations about this maximum power point.

4.2 Experimental Results for Low Solar Insolation

The performance of the MPPT for low solar insolation is shown in Fig. 8 Figs 8(a), 8(b), and 8(c) show output powers, integral value of output current V_{int}, and duty factor α, respectively. From the output power shown in Fig. 8(a), the proposed method tracks the maximum power point as quickly as that of the Hill climbing method does It is seen that the optimum operating point $\hat{\alpha}_{opt}$ is exactly estimated as shown in Fig 8(c), where $\hat{\alpha}_{opt}$ is close to 0.30 In this case, the proposed method can shorten the tracking time of MPPT without making any oscillations

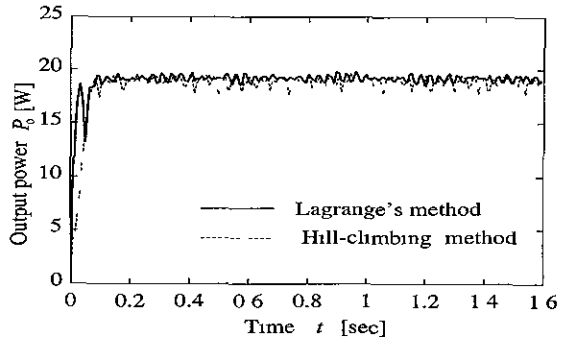

(a) Output power P_o

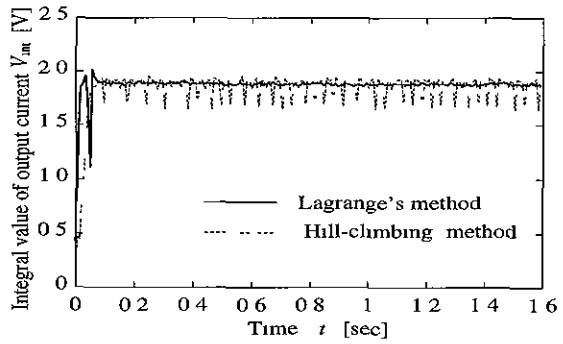

(b) Integral value of output current V_{int}

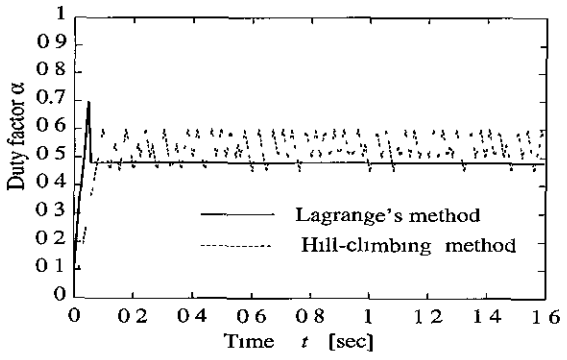

(c) Duty factor α

Fig 7 Maximum power point tracking performance for high solar insolation

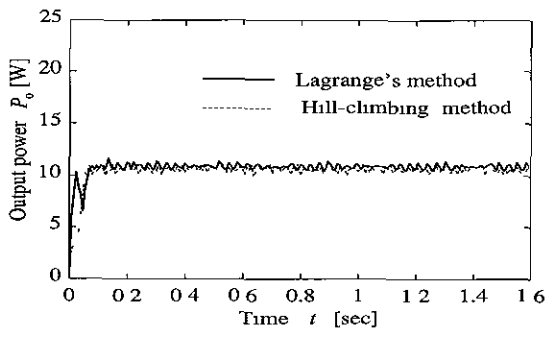

(a) Output power P_o

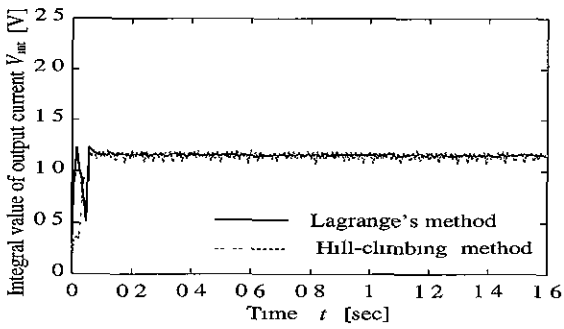

(b) Integral value of output current V_{int}

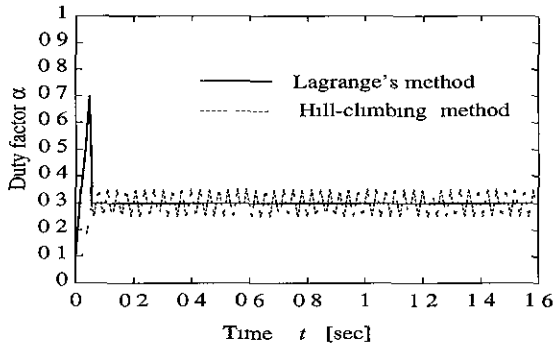

(c) Duty factor α

Fig 8 Maximum power point tracking performance for low solar insolation

4.3 Experimental Results for Stepwise Solar Insolation

Fig 9 shows the experimental results, for the case in which the solar insolation is changing in stepwise manner Figs 9(a), 9(b), and 9(c) show the output power, integral value of output current, and duty factor, respectively From the output power shown in Fig. 9(a), the proposed method tracks the maximum power point even if the solar insolation is changing

Therefore, when V_{int} reach at its maximum value, the output power moves close to the maximum power point as shown in Fig 9(a) From the above experimental results, it is demonstrated that the MPPT control using output current and the proposed algorithm can track the maximum power point quickly without making any oscillations about the operating point.

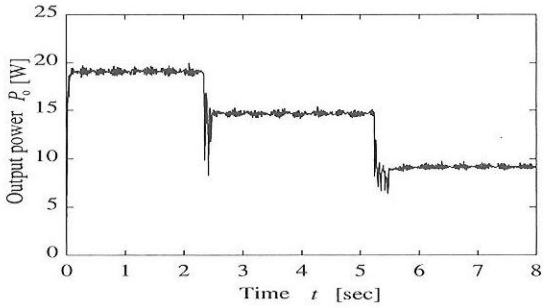

(a) Output power $P_{o.}$

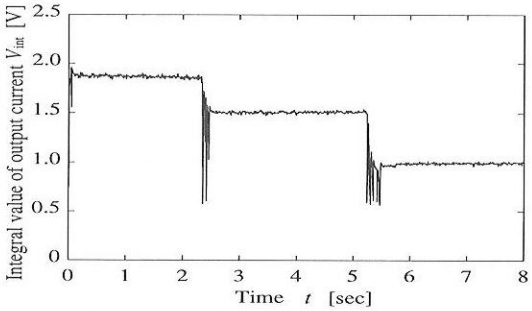

(b) Integral value of output current $V_{int.}$

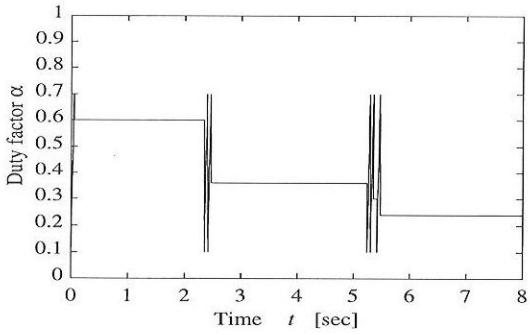

(c) Duty factor α.

Fig. 9. Maximum power point tracking performance for changing solar insolations.

5. Conclusion

A voltage sensorless maximum power point tracking algorithm is developed. In the proposed algorithm, the optimum operating point of PV array is estimated using output current information. The tracking effectiveness is demonstrated through experimental results. The experimental results show that the proposed algorithm tracks the maximum power point at a faster rate without showing any oscillations.

References

[1] S.J. Chiang, K.T. Chang, and et al., "Residential Photovoltaic Energy Storage System", *IEEE Transaction on Industrial Electronics*, Vol. 45, No. 3, pp. 385~394, 1998.

[2] Chihchiang Hua and Chihming Shen, "Comparative Study of Peak Power Tracking Techniques for Solar Storage System", *Proceedings of Applied Power Electronics Conference and Exposition* (APEC '98), Vol. 2, pp. 679~685, 1998.

[3] Jeong-Joon Ahn, Jae-Mun Kim, and et al., "A Study on DSP Controlled Photovoltaic System with Maximum Power Tracking", *Proceedings of International Conference on Power Electronics* (ICPE '98), pp. 966~971, 1998.

[4] Tomonobu Senjyu, Yasuyuki Arashiro, and Katsumi Uezato, "Maximum Power Point Tracking Control of Photovoltaic Array under Partial Shading Conditions", *The Transactions of The Institute of Electrical Engineers of Japan*, Vol. 119-B, No. 12, pp. 1331~1337, 1999.

[5] Tokuo Onishi and Shigeo Takata, "Comparisons of Maximum Power Tracking Strategy of Solar Cell Output and Control Characteristics using Step up/down Chopper Circuit", *The Transactions of The Institute of Electrical Engineers of Japan*, Vol. 112-D, No. 3, pp. 250~257, 1992.

[6] K.S. Lee, Y.J. Cho, and B.H. Cho, "Analysis of the Charge Controlled Inductor Current Sensing Peak-Power-Tracking Solar Array Regulator", *Proceedings of International Conference on Power Electronics* (ICPE '98), pp. 982~986, 1998.

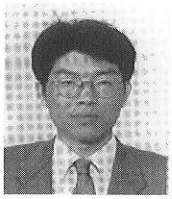

Tomonobu senjyu was born in Saga Prefecture, Japan, in 1963. He received the B.S. and M.S. degrees in electrical engineering from the University of the Ryukyus, Okinawa, Japan, in 1986 and 1988, respectively, and the Ph.D. degree in electrical engineering from Nagoya University, Nagoya, Japan, in 1944. Since 1988, he has been with the Department of Electrical and Electronics Engineering, Faculty of Engineering, University of the Ryukyus, where he is currently a professor. His research interests are in the areas of stability of ac machines, advanced control of electrical machines, and power electronics. Prof. Senjyu is a member of the Institute of Electrical Engineers of Japan.

Tomiyuki Shirasawa was born in Kagoshima Prefecture, Japan, in 1978. He received the B.S. degrees in electrical engineering from University of the Ryukyus, Okinawa, Japan, in 2001. Since 2001, he has been with the Department of Electrical and Electronics Engineering, Faculty of Engineering, University of the Ryukyus, where he is currently a master student. His research interests are in the areas of development of photovoltaic array system. Mr. Shirasawa is a student member of the Institute of Electrical Engineers of Japan.

Katsumi Uezato was born in Okinawa Prefecture, Japan, in 1940. He received the B.S. degrees in electrical engineering from the Univ. of the Ryukyus, Okinawa, Japan, in 1963, the M.S. degree in electrical engineering from Kagoshima Univ., Kagoshima, Japan, in 1983. Since 1972, he has been with the Dept. of Electrical and Electronics Engineering, Faculty of Engineering, Univ. of the Ryukyus, where he is currently a Professor. He is engaged in research on stability and control of synchronous machines. Prof. Uezato is a member of the IEEJ.

JPE 2-3-2

Voltage Sag Detection Algorithm for Instantaneous Voltage Sag Corrector

[1]Sanghoon Lee and [2]Jaeho Choi*

[1] POSCON Corporation, Seoul, Korea
[2] Chungbuk National University, CheongJu, Korea

ABSTRACT

Voltage sag detection algorithm for voltage sag corrector is proposed in this paper. To quantify the standard of voltage unbalance under the faulted conditions, the 3-phase unbalanced voltages are decomposed into two balanced 3-phase symmetrical components of the positive and negative sequence voltages, which is defined by the magnitude factor (*MF*) and unbalance factor (*UF*) It is analyzed that *MF* and *UF* values are given as the dc constant values even though under the voltage unbalance condition This paper also proposes the control scheme of the instantaneous voltage sag corrector based on this detection algorithm The validity of the proposed algorithm is verified through the EMTDC simulation and experiments.

Keywords· Instantaneous voltage sag corrector, Power quality, Magnitude factor, Unbalance factor

1. Introduction

The power quality problems due to a wide range of line disturbances, ranging from the voltage sags and swells to the harmonic distortions, become an important concern in the power distribution systems or the industrial power plants Among these line disturbances, the voltage sags are the most important power quality problems facing many industrial customers Voltage sag means the momentary decrease of voltage magnitude for duration of between 0 5 to 30 cycles[1][2] It is usually caused by a remote fault somewhere on the power system Customers living hundreds of miles away from the fault location can still experience the voltage sag resulting in the mal-operation of the power and control equipments when the fault is on the transmission system The large majority of the utility line faults are single line-to-ground faults (SLGF) SLGF's on the utility system is the most common cause of voltage sags in an industrial plant[3]

Voltage sags of short duration induce the fatal results to the high-technology electronic loads that are very sensitive to the deviations of the supply voltage Constant voltage transformers (CVT) or uninterruptible power supplies (UPS) are the common approach to mitigate or eliminate the voltage sag problems CVT's are easy and economic to install, but not efficient under the variable load condition or large inrush current condition UPS's are more excellent than CVT's, but these are costly, especially for larger ratings, have some frequent maintenance problems The instantaneous voltage sag correctors (IVSC) are more effective for maintaining the voltage within limits and balancing it Figure 1 shows the IVSC system using series voltage compensators Depending on the range and severity of faults to be handled, these may have ratings of

Manuscript received April 9, 2002, revised June 12, 2002.
Corresponding Author choi@power chungbuk ac kr, Tel +82-43-261-2425, Fax +82-43-276-7217

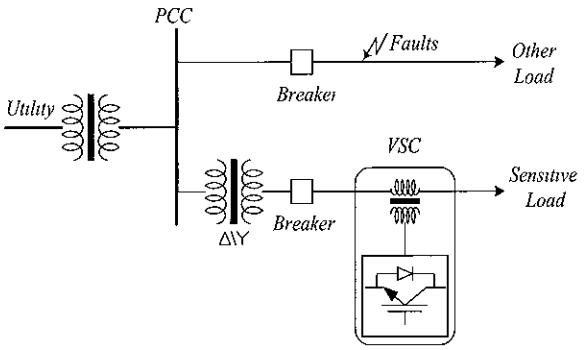

Fig 1 IVSC system in distribution line

only a fraction of the load This significantly reduces their cost comparing with the UPS solution In addition, under normal line conditions, the losses associated with the compensating operation are very small, since the injected voltage is zero and the load is supplied directly by the feeder[4][5].

Several power structures and control algorithms have appeared in the literature However, many are designed to correct small unbalances in the supply with harmonic free networks Also, they do not consider fault conditions in the distribution systems, which will more seriously affect the sags and unbalance For the application in the distribution systems, the voltage sag detection algorithm is very important, because the faulted voltage should be detected and compensated instantaneously to meet the on-line compensation The detection algorithm for faulted voltage has to meet the very short detection time and the robustness against the noise and transient change of the voltage The previous researches of faulted voltage detection method are classified as followings.

1) Averaging method
2) Single-phase relative error method
3) dq-transformation with synchronously rotating reference frame

The detection method of average value is robust against the noise and transients in the input voltage. It can detect the power source abnormality, but takes at least half period to detect the abnormality. To improve the drawbacks of the averaging method, the detection of instantaneous value has been considered using the relative ac error value But all variables described as the instantaneous ac values have time variant characteristics, so the analysis of power system and design of control variables are very complicate

If 3-phase ac values are transformed to dq-values with the synchronously rotating reference frame, the dq-values are given as the constant dc values in case of 3-phase balanced condition. Therefore, all the problems with the formal two methods can be overcome using this transformation, but it is only under the 3-phase balanced condition. Although they are transformed to dq-values, ac components are still remained under the unbalanced condition Also the control algorithm is complicated and is generated with coupling terms[8].

This paper proposes a novel detection algorithm of faulted voltages under the unbalanced condition To quantify the standard of unbalance under the fault conditions, the 3-phase unbalanced voltages are decomposed into two balanced 3-phase symmetrical components of the positive and negative sequence voltages, which is defined by the magnitude factor (*MF*) and unbalance factor (*UF*) It is analyzed that *MF* and *UF* values are given as the dc constant values even though unbalance condition This paper also proposes the control scheme of the instantaneous voltage sag corrector based on this detection algorithm.

The proposed algorithm has advantages as followings The duration time for detection is short and constant because it is not affected by the fault starting position. The control variables have time-invariant characteristics although it is under the unbalance conditions. The structure of the proposed controller is simpler than that of the previous algorithm based on the dq-transformation with the synchronously rotating reference frame

Finally the validity of the proposed algorithm is verified through the simulation and experiment. The simulation is accomplished by PSCAD/EMTDC and the prototype experimental system is implemented by using the digital signal processor (TMS320C31).

2. Detection of *MF* and *UF*

Instantaneous voltage sags are generally caused by the faults of short circuits on the distribution line Most faults are generated from the natural phenomenon such as lightning, weather condition, tree branch or animal contact, and insulation failures or human activity

All faults except three line-to-ground fault (TLGF) have 3 phase unbalanced and unsymmetrical condition. *MF* and *UF* are defined as shown (1)

$$|MF| = \frac{V_P}{V_{ref}} \tag{1a}$$

$$|UF| = \frac{V_N}{V_P} \tag{1b}$$

where, V_P is the positive sequence component, V_N is the negative sequence component and V_{ref} is the normal voltage before faults

The phase and line-to-line voltage of source is defined by (2) and (3) with the line voltage value, V to get the symmetrical components

$$v_{sa}(t) = \frac{V}{\sqrt{3}}\cos(wt + \theta_a) \tag{2a}$$

$$v_{sb}(t) = \frac{V}{\sqrt{3}}\cos(wt - \frac{2\pi}{3} + \theta_b) \tag{2b}$$

$$v_{sc}(t) = \frac{V}{\sqrt{3}}\cos(wt + \frac{2\pi}{3} + \theta_c) \tag{2c}$$

$$v_{s,ab}(t) = V\cos(wt + \frac{\pi}{6} + \theta_a) \tag{3a}$$

$$v_{s,bc}(t) = V\cos(wt - \frac{\pi}{2} + \theta_b) \tag{3b}$$

$$v_{s,ca}(t) = V\cos(wt + \frac{5\pi}{6} + \theta_c) \tag{3c}$$

To calculate *MF* and *UF* defined by (1), the symmetrical components should be calculated with the line voltage as shown by (4)

$$\begin{bmatrix} v_{s,abP} \\ v_{s,abN} \end{bmatrix} = \frac{1}{3}\begin{bmatrix} 1 & \alpha & \alpha^2 \\ 1 & \alpha^2 & \alpha \end{bmatrix}\begin{bmatrix} v_{s,ab} \\ v_{s,bc} \\ v_{s,ca} \end{bmatrix} \tag{4}$$

where, $\alpha = e^{J\frac{2\pi}{3}}$

As an example of faults, SLGF is considered as followings: If SLGF is happened in a-phase, the phase voltage of 'a' will be zero, and the line-to-line voltages of (3) will be given to (5)

$$v_{s,ab}(t) = -\frac{V}{\sqrt{3}}\cos(wt - \frac{2\pi}{3} + \theta_b) \tag{5a}$$

$$v_{s,bc}(t) = V\cos(wt - \frac{\pi}{2} + \theta_b) \tag{5b}$$

$$v_{s,ca}(t) = \frac{V}{\sqrt{3}}\cos(wt + \frac{2\pi}{3} + \theta_c) \tag{5c}$$

Equation (5) shows that $v_{s,bc}$ is same regardless of faults but the magnitudes of the other two decrease to 58[%] and the phase is shifted ±30[°] By substituting (5) to (4), we can get the symmetrical components as shown in (6)

$$\begin{bmatrix} v_{s,abP} \\ v_{s,bcP} \\ v_{s,caP} \end{bmatrix} = T_P \quad v_{s,abP} = \frac{2V}{3}\begin{bmatrix} \cos(\omega t + \frac{\pi}{6} + \theta) \\ \cos(\omega t - \frac{\pi}{2} + \theta) \\ \cos(\omega t + \frac{5\pi}{6} + \theta) \end{bmatrix} \tag{6a}$$

$$\begin{bmatrix} v_{s,abN} \\ v_{s,bcN} \\ v_{s,caN} \end{bmatrix} = T_N \quad v_{s,abN} = \frac{V}{3}\begin{bmatrix} \cos(\omega t + \frac{5\pi}{6} + \theta) \\ \cos(\omega t - \frac{\pi}{2} + \theta) \\ \cos(\omega t + \frac{\pi}{6} + \theta) \end{bmatrix} \tag{6b}$$

where, $T_P = \begin{bmatrix} 1 & \alpha^2 & \alpha \end{bmatrix}^T$ and $T_N = \begin{bmatrix} 1 & \alpha & \alpha^2 \end{bmatrix}^T$.

By comparing (6) with (3), it is known that the magnitudes of positive sequence component decrease to 66.7[%] and their phase are same And the magnitudes of negative sequence component decrease to 33.3[%] and the phase sequence is opposite to that in the positive sequence while the phase of $v_{s,bc}$ is same as that of the normal voltage. Therefore, *MF* for 3 line voltages is dc value of 0 667 and only *UF* for bc line voltage is dc value of 0 5 Table I shows the magnitude of *MF* and *UF* values for some kinds of faults. If the fault impedance is zero, *MF* and *UF* have the time invariant characteristics as shown in Table 1

Table 1 *MF* and *UF* under faults

	SLGF	LLF	DLGF	TLGF
MF	0.667	0.5	0.333	0
UF	0.5	-1	-1	0

3. Detection Algorithm

As shown in Fig 1, the purpose of IVSC system is to protect the sensitive load against the instantaneous voltage sag caused by the distribution line fault So IVSC system has the capability of real time compensation and its power failure detection algorithm should be designed to suitable for real time control

The detection algorithm is very important for the operation of IVSC system, because this works not only to detect the faulted voltage but also to determine the operating point of the system In case of the detection algorithm which is implemented at existing synchronous coordinator, the fault-starting-point affects the total detecting time because the algorithm has a time variant characteristic under three phase unbalanced condition As a result, the system may not be real time compensation. In this paper, to overcome the above disadvantage a new detection algorithm based on the *MF* as described in chapter 2 is proposed

Fig 2(a) shows an overall block diagram of the fault voltage detection part and it is detailed in Fig. 2(b) A basic digital filter is used to get the robust characteristics against the noise included in the feedback signal and the transients of source But the phase delay problem is evitable with this filter and it affects adversely the performance of the instantaneous detection and control algorithm.

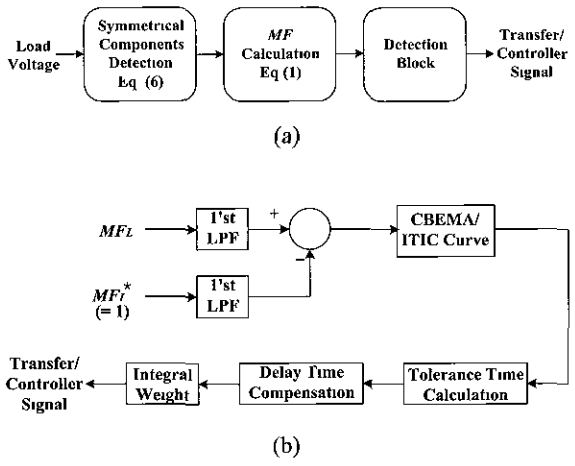

Fig 2 Proposed detection algorithm (a) Overall block diagram (b) Detailed scheme of detection block in (a)

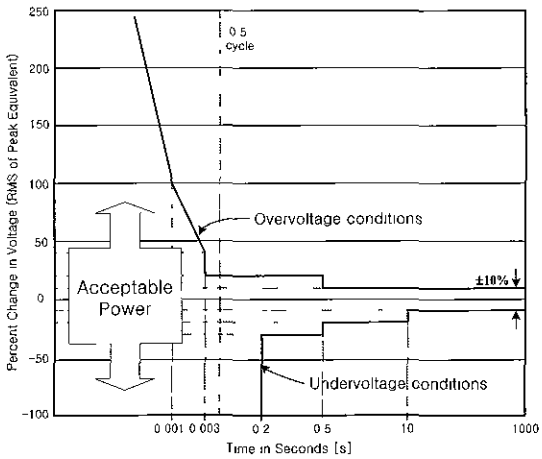

Fig 3 ITIC vurve

The ITIC (Information Technology Industry Council) curve in Fig 3 is used as the standards of power state So the switch transfer and the compensation action would be carried out under the toleration time[6]

The proposed detection algorithm has many advantages for the previous that First, it is available to a fast and precise detection regardless of the point when fault begins. It is means that the *MF* is represented as a DC value for the various faults. Second, the control algorithm, which is implemented by the proposed detection algorithm, has a time invariant characteristic, so the design and structure is very simple

4. Control Algorithm

The general requirements for IVSC system are as followings; fast dynamic response, robustness for noise, and isolation from harmonics In this paper, the last requirement is not considered The configuration of power circuit and the proposed control block diagram are shown in Fig 4 and Fig 5 Under the fault condition, the controller operates to keep the load voltage constant. Otherwise, the controller doesn't work but only the dc capacitor is charged from the source.

As shown in Fig 5, this paper proposes the novel control algorithm for IVSC system based on the proposed detection algorithm In these figures, the subscript S, L and C mean the source, load, and the compensator.

So, using IP controller, the *MF* and *UF* of compensation voltage is controlled Consequently the basic control structure is the instantaneous control of the inverter output

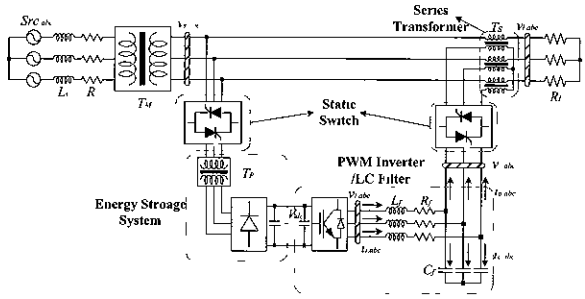

Fig 4 Configuration of power circuit for IVSC

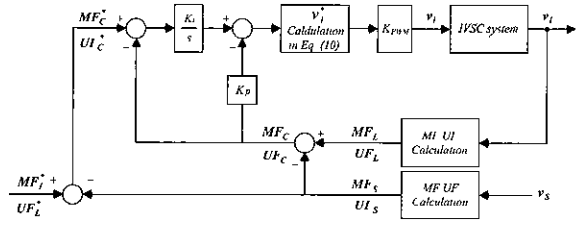

Fig 5 Proposed control algorithm

capacitor voltage For the purpose of dynamic characteristic improvement of controller, the inner current control loop of inductor could be added, but in this paper did not use it

One of the important things for the voltage compensation is how to determine the reference value of the compensator output voltage calculated by the following steps from Fig. 4 and Fig 5 In Fig. 4, the reference value of the compensator output voltage is described to be able to compensate the voltage difference between the reference load voltage and the faulted source voltage as followings

$$\left[v^{*}_{c,abc}\right] = \frac{1}{K_T}\left\{\left[v^{*}_{l,abc}\right]-\left[v_{s,abc}\right]\right\} \tag{7}$$

where, $[v_{abc}]=[v_{ab}\ \ v_{bc}\ \ v_{ca}]^T$ and K_T is the winding ratio of the series transformer

And also, the positive and negative sequence components of the reference inverter voltage are given by (8)

$$\left[v^{*}_{c,abc}\right]_P = \frac{T_P}{K_T}\left\{\left[v^{*}_{la,P}\right]-\left[v_{sa,P}\right]\right\} \tag{8a}$$

$$\left[v^{*}_{c,abc}\right]_N = \frac{T_P}{K_T}\left\{\left[v^{*}_{la,N}\right]-\left[v_{sa,N}\right]\right\} \tag{8b}$$

For the control of the voltage sag compensation under the unbalance and unsymmetrical power condition, the ideal values of the positive and negative sequence components of the load voltage is given by the reference voltage value, v_{ref}, and zero, respectively. By substituting these values in (8), the reference values of the positive and negative sequence components of the compensator output voltage are given as followings

$$\left[v^{*}_{c,abc}\right]_P = \frac{T_P}{K_T}\left(1-\frac{v_{sa,P}}{v_{ref}}\right)v_{ref} \tag{9a}$$

$$\left[v^{*}_{c,abc}\right]_N = -\frac{T_P}{K_T}\frac{v_{sa,N}}{v_{ref}}v_{ref} \tag{9b}$$

Then, by substituting (1) into (8) the compensator output voltage is described simply by (10)

$$\left[v^{*}_{c,abc}\right]_P = \frac{T_P}{K_T}(1-MF_S)v_{ref} \tag{10a}$$

$$\left[v^{*}_{c,abc}\right]_N = -\frac{T_P}{K_T}MF_S\ UF_S\ v_{ref} \tag{10b}$$

If we ignore the voltage drop at R_f, the reference voltage of inverter output will be the same value of the compensator output v_c^* and can be written as (11)

$$\left[v^{*}_{i,abc}\right] = K_{PWM}\left\{\left[v^{*}_{c,abc}\right]_P+\left[v^{*}_{c,abc}\right]_N\right\} \tag{11}$$

5. Simulation and Experimental Results

To verify the validity of the proposed algorithm, the simulation and experimental results are given as followings. The simulation is accomplished by PSCAD/EMTDC using the parameters given in Table 2 All the variables are shown as per unit values and the voltage values in Table 2 are peak value of phase voltage

Table 2 Simulation parameters

Parameter	Value	Parameter	Value
Power rating	10[kVA]	Switching frequency	5[kHz]
Voltage	311[V]	Faults duration	60[ms]
Current	37 1[A]	Winding ratio (T_S)	1 1